https://doi.org/10.5194/essd-2023-535
Preprint. Discussion started: 2 February 2024

Open Access Earth System Science Data Discussions

Calving front positions for 19 key glaciers of the Antarctic Peninsula: a sub-seasonal record from 2013 to 2023 based on a deep learning application to Landsat multispectral imagery

Erik Loebel[1], Celia A. Baumhoer[2], Andreas Dietz[2], Mirko Scheinert[1], and Martin Horwath[1]

[1]Technische Universität Dresden, Institut für Planetare Geodäsie, Dresden, Germany
[2]German Aerospace Center, Earth Observation Center, Weßling, Germany

Correspondence: Erik Loebel (erik.loebel@tu-dresden.de)

Abstract. Calving front positions of marine-terminating glaciers are an essential parameter to understanding dynamic glacier changes and constraining ice modelling. In particular, for the Antarctic Peninsula, where the current ice mass loss is driven by dynamic glacier changes, accurate and comprehensive data products are of major importance. Current calving front data products are limited in coverage and temporal resolution because they rely on manual delineation being time-consuming and unfeasible for the increasing amount of satellite data. To simplify the mapping of calving fronts we apply a deep learning based processing system designed to automatically delineate glacier fronts from multispectral Landsat imagery. The U-Net based framework was initially trained on 869 Greenland glacier front positions and is here extended by 236 front positions of the Antarctic Peninsula. The here presented data product includes 2064 calving front locations of 19 key outlet glaciers from 2013 to 2023 and achieves sub-seasonal temporal resolution. This data set will help to better understand marine-terminating glacier dynamics on an intra-annual scale, study ice-ocean interactions in more detail and constrain glacier models. The data is publicly available at PANGAEA under https://doi.pangaea.de/10.1594/PANGAEA.963725 (Loebel et al., 2023b).

1 Introduction

From 1992 to 2020 the Antarctic Ice Sheet lost $2671 \pm 530\,\mathrm{Gt}$ of ice, raising the global sea level by $7.4 \pm 1.5\,\mathrm{mm}$ (Otosaka et al., 2023). Mass loss is dominated by ice-dynamic processes, where warming ocean temperatures and the collapse of ice shelves reduce buttressing and accelerate ice flow (Slater et al., 2020). At the Antarctic Peninsula (AP) in particular, increasing ice loss has been linked with ice shelve disintegration (Rott et al., 1996; Rignot et al., 2004; Cook and Vaughan, 2010; Adusumilli et al., 2018; Rack and Rott, 2004). Forcing from ocean (Cook et al., 2016) and atmosphere (Vaughan and Doake, 1996; Cook et al., 2005; Cape et al., 2015) has led to reduced ice shelf thickness and extent. And this, in turn, has reduced buttressing strength and thereby increased outlet glacier dynamics and ice discharge (Rignot et al., 2004; Rott et al., 2018; Seehaus et al., 2018; Wallis et al., 2023a). Hence, it is of utermost importance to monitor AP glaciers and ice shelves to come up with up-to-date diagnostics and reliable predictions of future change.

One particularly important parameter of each glacier is the calving front position and its temporal variation. Calving front locations are essential for (1) mapping glacier area change (Davies et al., 2012); (2) studying and understanding ice-ocean

https://doi.org/10.5194/essd-2023-535
Preprint. Discussion started: 2 February 2024

Table 1. Overview of publicly available calving front data sets for the AP. The number of mapped fronts in (Cook et al., 2021) is not documented. It is specified that more than 2000 aerial photographs and over 100 satellite images were used to compile the dataset.

Dataset	Annotation	Sensor type	Glaciers	Mapped fronts	Time span
ADD (Cook et al., 2021)	Manually	Optical	244		1843-2008
GLIMS (GLIMS Consortium, 2005)	Manually	Optical	>300	>900	Since 1986
Seehaus et al. (2015)	Manually	SAR	1	147	1992-2014
Seehaus et al. (2016)	Manually	SAR	1	133	1993-2014
CryoPortal (ENVEO)	Manually	SAR & Optical	16	124	2013-2017
Lippl (2019)	Manually	Optical	26	656	2014-2018
Gourmelon et al. (2022)	Manually	SAR	5	457	1996-2020
Wallis et al. (2023b)	Manually	SAR	8	3430	2015-2021
This study (Loebel et al., 2023b)	Automatic	Optical	19	2604	2013-2023

interaction as well as underlying processes (Scambos et al., 2011; Seehaus et al., 2015, 2016); and (3) constraining ice-dynamic models to improve simulations of future mass loss and sea level contribution (Alley et al., 2005; Barrand et al., 2013; Cornford et al., 2015). Accurate calving front data with both high temporal resolution and a high spatial coverage is therefore critical. These data products are not widely available for the AP. This is due to limitations of the manual and therefore time-consuming, process of delineating these frontal positions from the increasing amount of satellite imagery available.

Table 1 gives an overview of publicly available calving front data sets for the AP. The Antarctic Digital Database (ADD) and Global Land Ice Measurements from Space (GLIMS) products have circum-Antarctic coverage but very limited temporal resolution. The calving front data by Seehaus et al. (2015), Seehaus et al. (2016), Lippl (2019) and Wallis et al. (2023b) are by-products of regional glaciological studies. Calving fronts reported by Gourmelon et al. (2022) are part of a benchmark dataset developed for evaluating automated extraction from SAR imagery. The availability of calving front positions at the AP is limited, emphasising the necessity for additional and more comprehensive data products. For this, we need to use automatic annotation methods.

In recent years, deep learning has emerged as the tool of choice to accomplish this task (Mohajerani et al., 2019; Baumhoer et al., 2019; Zhang et al., 2021; Heidler et al., 2021; Marochov et al., 2021; Periyasamy et al., 2022; Davari et al., 2022b, a; Heidler et al., 2022; Herrmann et al., 2023). This has already been demonstrated by Baumhoer et al. (2023), who applied neural networks on SAR imagery to generate a high temporal resolution dataset of Antarctic ice shelf frontal positions. On the AP this IceLines data set (Baumhoer et al., 2023) solely encompasses the Larsen Ice Shelf and excludes the outlet glaciers. Similar methods have been used to generate calving front data products for outlet glaciers in Greenland (Cheng et al., 2021; Zhang et al., 2023; Loebel et al., 2023c) and Svalbard (Li et al., 2023).

With this contribution, we provide a dense calving front data product for 19 key glaciers of the AP. We achieve this by applying a processing system, initially developed for Greenland, and incorporating new reference data. The locations of these

https://doi.org/10.5194/essd-2023-535
Preprint. Discussion started: 2 February 2024

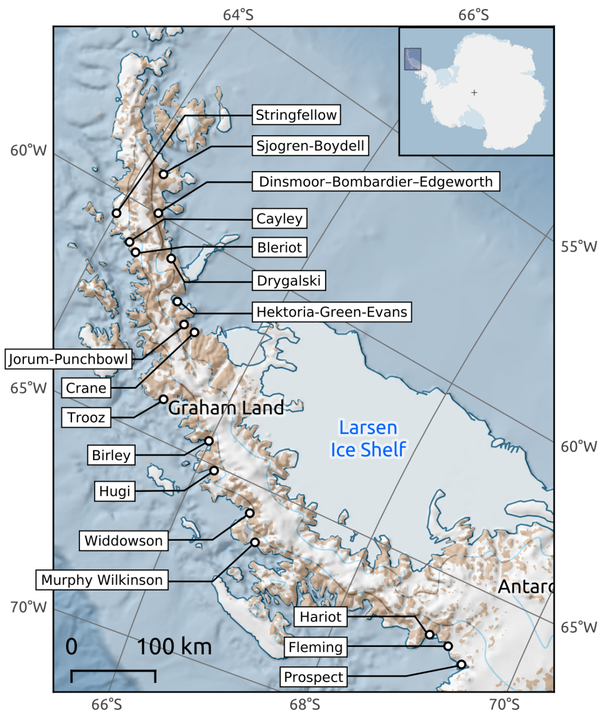

Figure 1. Overview map of the Antarctic Peninsula and the 19 glaciers included in the presented data product. The Larsen Ice Shelf is part of the IceLines (Baumhoer et al., 2023) data set.

glaciers are shown in Figure 1, and the period covered ranges from 2013 to 2023. Glaciers were chosen for their glaciological importance, mass balance and size. Mainly, our data incorporates the glaciers and former ice shelf tributaries of the two sub-regions Larsen-A and -B (east coast of the northern AP) as well as Wordie Bay – the two major hotspots of ice loss at the AP. Our data for Larsen-A and -B area includes the glaciers Crane, Jorum, Punchbowl, Hektoria-Green-Evans, Drygalski, Dinsmore-Bombardier-Edgeworth, Sjogren and Boydell. For Wordie Bay we provide data for the glaciers Hariot, Fleming and Prospect. The Fleming, Drygalski and Hektoria-Green-Evans glaciers alone account for almost 40 % of the total mass loss in our processing area from 2013 to 2017 (Seehaus et al., 2023). Driven by ice shelf disintegration, glaciers in these two sub-regions have undergone recent changes in ice dynamics, elevation, and calving front retreat (Seehaus et al., 2018; Friedl et al., 2018; Rott et al., 2018). The remaining glaciers in our data set (Murphy Wilkinson, Widdowson, Hugi, Birley, Trooz, Bleriot, Cayley and Stringfellow), all located on the west coast of the AP, were selected based on the relatively large size of their calving front.

https://doi.org/10.5194/essd-2023-535
Preprint. Discussion started: 2 February 2024

Open Access Earth System Science Data Discussions

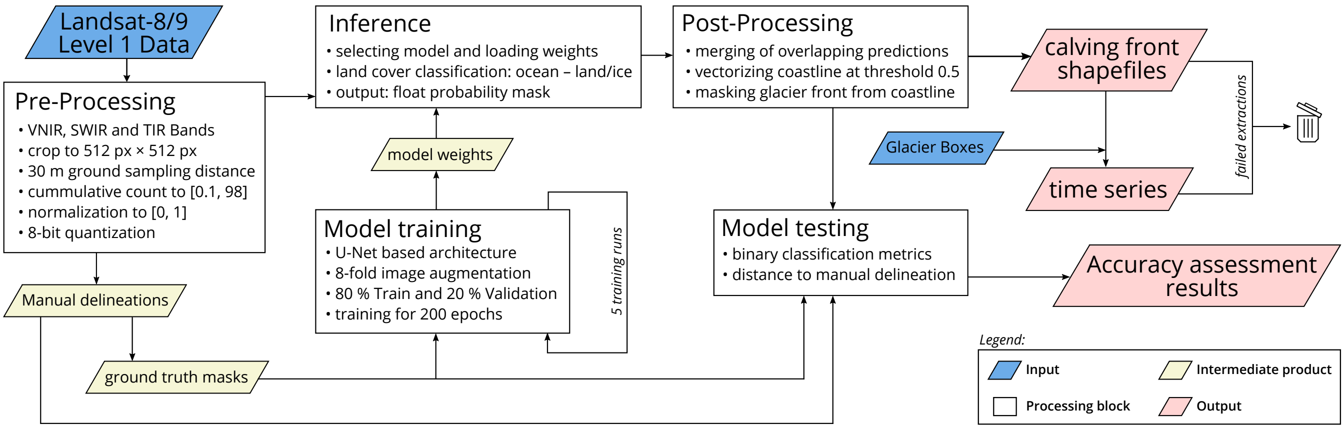

Figure 2. The workflow of the applied processing system divided into the various processing blocks.

2 Methods

The processing is based on the method previously described in Loebel et al. (2023c). Originally developed for marine-terminating outlet glaciers in Greenland, the method is built with a high degree of automatization. The only modification applied to the framework is the extension of the reference dataset to incorporate glaciers on the AP. Figure 2 gives a comprehensive overview of the processing system. The steps involved are briefly described below, followed by an accuracy assessment of the results.

2.1 Calving front delineation by deep learning

Our processing is based on multispectral Landsat-8 and Landsat-9 Level-1 data. During pre-processing nine available satellite bands, ranging from visible and infrared (VNIR) over short-wave infrared (SWIR) to thermal infrared (TIR), are cropped into 512 px $\times$ 512 px tiles with a unified ground sampling distance of 30 m, centered at the corresponding calving front. To counteract image overexposure we apply a cumulative count cut image enhancement, clipping the data between the 0.1 and 98 percentile. Furthermore, all bands are normalized between 0 and 1 by a 8-bit quantization. Ground truth reference was inferred by manual delineation for both training and testing our Artificial Neural Network (ANN). To train the model we apply 869 Greenland calving front positions and additional 236 calving fronts from 11 AP glaciers. Due to the similar morphology of Greenland and AP outlet glaciers, these 869 Greenland calving front positions represent an ideal basis for a well-generalized ANN model. The additional AP 11 glacier are Jorum, Punchbowl, Prospect, Hektoria-Green-Evans, Dryglaski, Birley, Crane, Widdowson, Fleming, Sjogren and Boydell. Expanding the training data set is beneficial to account for the partly different glacier morphology, such as the presence of free-floating glacier tongues. To avoid model overfitting, we make sure that the training data covers different calving and ice mélange conditions, as well as varying illumination, cloud situations.

The applied ANN performs a land cover classification where an ocean class is semantically segmented from a glacier/land class. In particular we use a modified U-Net (Ronneberger et al., 2015) with two additional contracting and expanding blocks.

https://doi.org/10.5194/essd-2023-535
Preprint. Discussion started: 2 February 2024

This modification results in a larger receptive field which is helpful for calving front extraction (Heidler et al., 2021). 20 % of the input data is used for internal model validation and model selection. Training data is augmented eight times by rotation and mirroring. For model training, we used the Adam optimization algorithm (Kingma and Ba, 2014) on a binary cross-entropy loss function for 200 epochs and randomized batches of size eight. The model output is a floating point probability mask. Each image pixel is assigned a probability between 0 (water) and 1 (glacier and land). Since the terminus length of the Hektoria-Green-Evans glacier system exceeds the fixed window size, we infer five separate but partially overlapping predictions here. We then merge these five predictions by averaging the values where they overlap. During post-processing the prediction is vectorized using the Geospatial Data Abstraction Library (GDAL/OGR contributors, 2020). The glacier front is then extracted from the predicted coastline using a static mask.

For further analysis and illustration, the calving front location shape-files are processed using the rectilinear box method (Moon and Joughin, 2008). We use this method not only to generate the time series of terminus area change but also to remove failed calving front extractions. For this we separate all entries that have an area difference of more than $1\,\mathrm{km}^2$ from the previous and following entries. Separated entries are checked manually.

2.2 Accuracy assessment

The accuracy of the data product is estimated by comparing automated calving front extractions to manual delineations. In Loebel et al. (2023c), the processing system has already been validated for accuracy and generalizability, with particular emphasis on Greenland Glaciers. Since we use additional training data for this analysis, we also apply a manually delineated test data set specifically for the AP. This test data set contains 57 calving front locations over all 19 processed glaciers. This includes additional eight glaciers which are not part of the training data set. These additional eight test glaciers ensure the spatial transferability of our method. Whereas the training data contains calving fronts from 2013 to 2021, the test data set contains calving fronts for the separate period from 2022 and 2023. As ANN training is not deterministic, we train five separate models for our assessment. Our main error metric is the distance between the predicted delineation and the manual delineation. This is implemented by averaging the minimum distance every $30\,\mathrm{m}$ along the predicted front trajectory.

Figure 3 shows test images for a diverse range of challenging conditions concerning ice mélange, cloud cover, iceberg presence, low illumination and satellite scene borders. Our processing system reliably delineates calving fronts from images with a wide range of ocean, ice mélange and illumination conditions. Furthermore, the ANN is able to handle images affected by light cloud cover as well as images with calving fronts near the edge of a satellite scene. This is due to the large training data set, which covers a wide variety of satellite images under these conditions. In addition, the integration of multispectral input data leads to more accurate predictions under these difficult situations (Loebel et al., 2022). The largest mean distance errors occur on glaciers with frequent calving events (e.g. Fleming glacier or Prospect glacier), where it is difficult to distinguish icebergs from the crevassed glacier terminus. Within the entire test data set, 49 out of 57 calving front predictions have an assessed accuracy of better than $100\,\mathrm{m}$.

Table 2 gives an overview of the accuracy assessment over the entire test dataset. In addition to mean and median distance to manual delineation, we also specify the binary classification metrics accuracy, precision, recall and F1-Score. Whilst a high

https://doi.org/10.5194/essd-2023-535
Preprint. Discussion started: 2 February 2024

Open Access Earth System Science Data Discussions

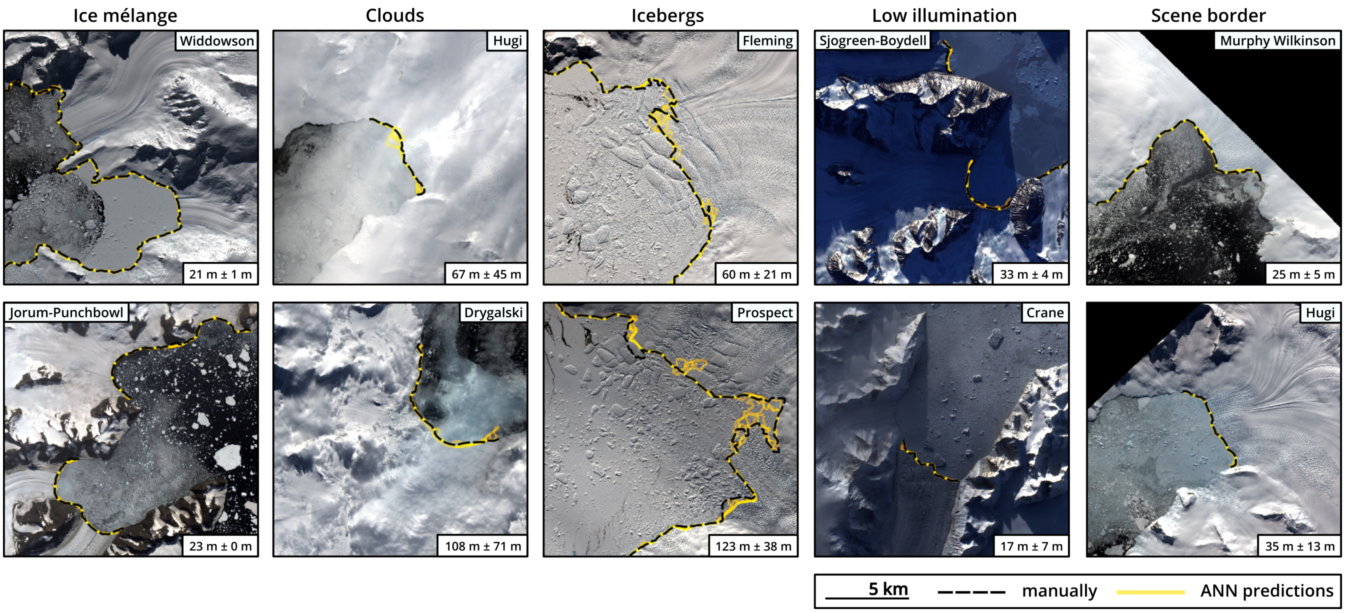

Figure 3. Accuracy assessment results of sample scenes from the test data set for challenging conditions concerning ice mélange, cloud cover, iceberg presence, low illumination and satellite scene borders. Dashed black lines show manually delineated calving fronts. Yellow lines show the five ANN predictions from five models. Overlap of lines is indicated by higher color intensity. The mean distance error for each scene is given in meters. For location of specific glaciers, see Figure 1. Landsat imagery courtesy of the U.S. Geological Survey.

Table 2. Results of the accuracy assessment presented as mean values with corresponding standard deviations calculated over the five trained models. The mean and median distance to manual delineation as well as accuracy, precision, recall and F1-Score are given. Binary classification metrics relate to the land/glacier class.

Distance to manual delineation		Binary classification metrics			
Mean (m)	Median (m)	Accuracy	Precision	Recall	F1-Score
59.3 ± 5.9	33.9 ± 1.5	0.984 ± 0.001	0.978 ± 0.002	0.995 ± 0.001	0.986 ± 0.001

binary classification performance does not necessarily translate to an accurate prediction of the calving front trajectory, we report these values to facilitate comparability of our results with other studies and datasets. Although completely different test data sets are involved, the $59.3 \pm 5.9\,\mathrm{m}$ mean distance error calculated here aligns very well with the $61.2 \pm 7.5\,\mathrm{m}$ reported by Loebel et al. (2023c). Importantly, it is below the accuracy level of manual digitization, which Goliber et al. (2022) reported to be $107\,\mathrm{m}$ based on duplicated delineations from different authors.

When assessing the accuracy only for the 23 test scenes of glaciers outside the training dataset we calculate a mean delineation error of $51.9 \pm 6.7\,\mathrm{m}$ (median: $37.3 \pm 5.3\,\mathrm{m}$). Interestingly, this is a lower mean and higher median error compared to an assessment over the 34 scenes from glaciers within the training dataset, where we estimate a mean delineation error of

https://doi.org/10.5194/essd-2023-535
Preprint. Discussion started: 2 February 2024

Table 3. Temporal coverage of our ANN generated time series. The numbers and the color intensity indicate the amount of processed calving front positions in the respective year.

	Jorum	Punchbowl	Prospect	Hektoria-Green-Evans	Drygalski	Birley	Bleriot	Crane	Edgeworth	Hugi	Murphy Wilkinson	Stringfellow	Trooz	Widdowson	Cayley	Fleming	Hariot	Boydell	Sjogren	
2013	5	5	8	2	2	7	4	5	3	7	6	4	7	7	4	9	10	3	3	
2014	9	9	13	11	17	13	12	10	16	14	21	12	14	12	12	14	13	14	14	
2015	12	12	15	12	18	11	15	14	20	12	11	15	11	9	14	15	15	17	17	
2016	14	14	11	15	21	11	11	18	17	13	17	11	10	11	10	11	10	11	11	
2017	13	13	13	9	16	11	13	14	17	10	10	11	10	8	11	13	14	15	15	
2018	19	19	11	9	15	10	8	17	10	14	15	6	11	11	8	13	16	15	15	
2019	10	10	15	7	16	13	13	9	15	13	22	8	11	13	14	17	12	13	13	
2020	14	14	7	10	21	15	13	18	19	14	19	8	17	12	8	8	9	15	15	
2021	17	17	10	13	32	13	6	22	21	11	13	12	13	9	9	13	12	18	18	
2022	17	17	18	16	35	11	7	24	21	15	21	13	15	13	8	20	20	27	27	
2023	8	8	6	5	13	6	5	12	13	7	8	3	4	6	4	5	6	10	10	
Total	138	138	127	109	206	121	107	163	172	130	163	103	123	111	102	138	137	158	158	2604

65.3 ± 7.7 m (median: 33.8 ± 1.5 m). This is because of training glaciers that have challenging-to-delineate calving conditions (like Prospect Glacier, see Fig. 3). Based on these numbers, we confirm the high degree of ANN model generalization and hence the spatial transferability of our method.

3 Data product and usage notes

The data product presented here has been created to provide glaciologists and glacier modellers with high quality calving front positions of the AP without the need for manual delineation. Figure 1 gives a spatial overview of the 19 processed glaciers. These glaciers have been selected on the basis of their glaciological significance, in particular their mass balance, retreat rate, size and flow velocity. A tabular overview is given in Table 3. In total the data record encompasses 2604 calving front positions. Since the data is derived from optical imagery, the time series have a 14-week gap during polar night from May to mid-August. Outside polar night, on average the data set has one entry every 19.5 days. However, the sampling is irregular and primarily dependent on the satellite orbit and cloud cover. The time frame from 2013 to 2023 covers that of the IceLines dataset (Baumhoer et al., 2023), facilitating a combined analysis of circum-Antarctic calving front change.

Figure 4 gives seven example time series of terminus area change within two regions of the AP. The terminus area change of glaciers in the Larsen-B embayment (Fig. 4 a-d) is spatially correlated and shows a steady advance from 2013 until the end of 2021. At the beginning of 2022, our data show a simultaneous retreat of the four glaciers. Subsequently, the glacier tongues of Hektoria-Green-Evans, Jorum, and Crane glacier have collapsed. The dramatic retreat of these glaciers is shown for the first time in such high temporal resolution. This simultaneous retreat is attributed to the disintegration of landfast sea ice inside the embayment in early 2022 and the resulting loss of buttressing (Ochwat et al., 2023). The glaciers in Wordie Bay (Fig. 4 e-g) show a more varied calving front dynamics. These range from stable calving front positions (Hariot Glacier since mid 2020) over steady terminus advance superimposed by frequent calving events (Fleming Glacier) to large calving events (Prospect

https://doi.org/10.5194/essd-2023-535
Preprint. Discussion started: 2 February 2024

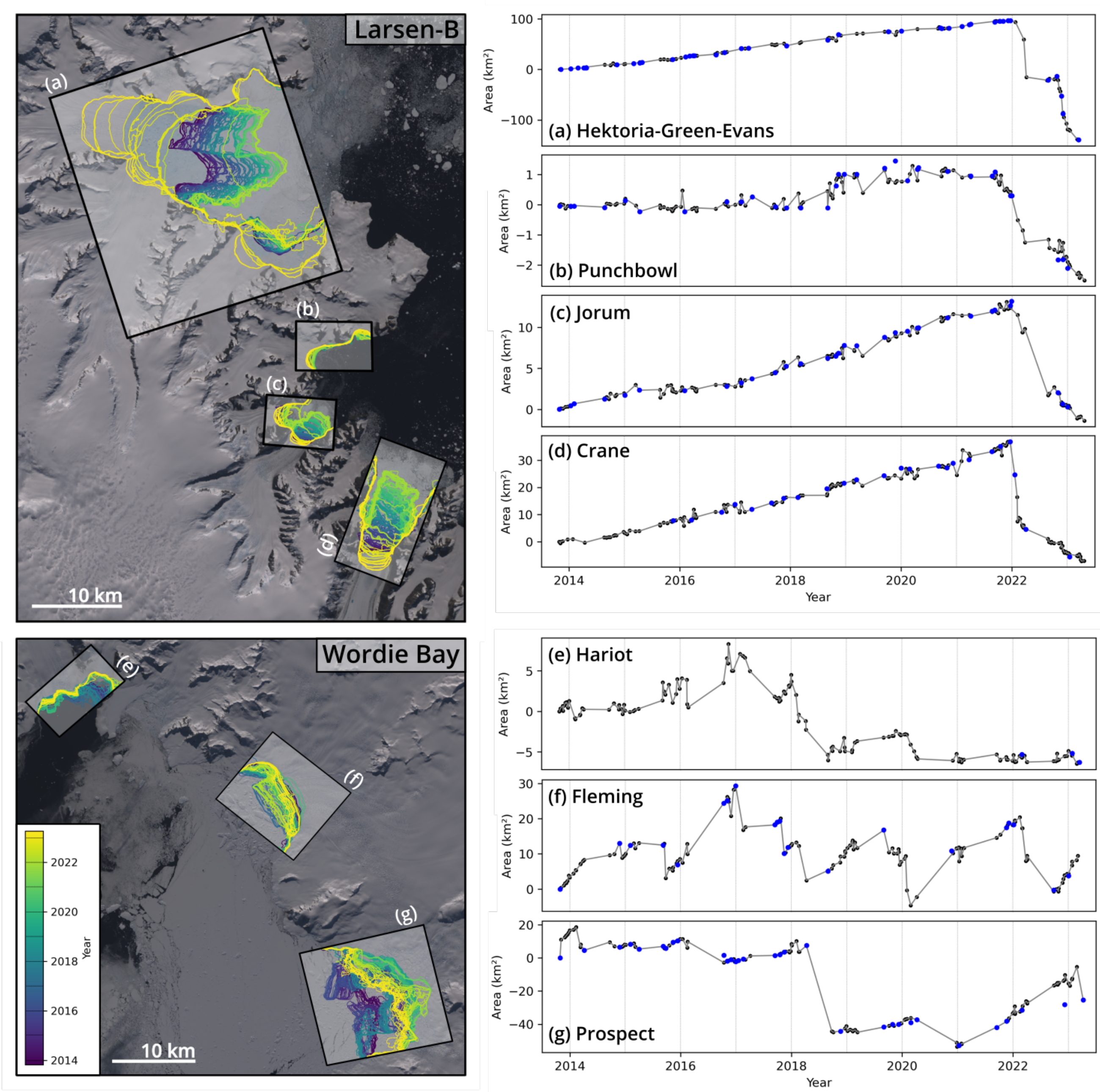

Figure 4. Example time series of terminus area change generated by our processing system for (a-d) four AP glacier in the Larsen-B embayment and for (e-g) three glaciers at Wordie Bay. Color-coded calving front locations are depicted in the maps in the left. Corresponding time series are shown on the right with entries marked by black dots. The blue dots are additional validation marks that indicate the frontal positions of the manually delimited reference data set. Landsat imagery courtesy of the U.S. Geological Survey.

https://doi.org/10.5194/essd-2023-535
Preprint. Discussion started: 2 February 2024

Glacier in 2018). The reason for this increased glacier dynamics is due to the disintegration of the Wordie Ice Shelf by the late 1990s. This has led to an increased ice flow and calving of the three main tributary glaciers Hariot, Fleming and Prospect (Friedl et al., 2018). Therefore, an operational and temporally high resolution monitoring of these glaciers is particularly important. An overview of the the time series of all 19 glaciers of our data product ins given in Figure S2 and Figure S3 in the supplement.

The glacier calving front locations are stored in linestring shapefiles, sorted by glacier and date within a file system structure. All shapefiles are georeferenced using the Antarctic Polar Stereographic Projection (EPSG:3031). This allows an easy handling e.g. by means of GIS software or geospatial data libraries. Additionally to the calving front location we also provide the entire coastline prediction. This facilitates the combination of the calving front with an overlapping ice mask. The file naming convention for each entry is: *[glacier name]_[YYYYMMDD]_[type].shp*. An example entry would be: *jorum_20230423_coastline.shp*. The attribute table of each file includes the glacier name, calving front date, type, processing date and processing version number.

4 Data and code availability

The AP calving front location data record is publicly available at PANGAEA under https://doi.pangaea.de/10.1594/PANGAEA.963725 (Loebel et al., 2023b). The calving front locations can be downloaded separately for each glacier by clicking on the "View Dataset as HTML" button in the overview. We provide a containerized implementation (platform: Docker) of the presented processing system. The software automatically extracts calving front positions from Landsat-8 or Landsat-9 Level-1 data archives for glaciers used within this study or at user-defined coordinates. This enables the analysis of glaciers that are outside our reference data set or beyond the temporal frame of our study. The software is available at https://github.com/eloebel/glacier-front-extraction (last access 20 December 2023) and https://doi.org/10.5281/zenodo.7755774 (Loebel, 2023a). Our implementation (software: Python 3) of the rectilinear box method is available at https://github.com/eloebel/rectilinear-box-method (last access 20 December 2023) and https://doi.org/10.5281/zenodo.7738605 (Loebel, 2023b). The processed time series of terminus area change, provided in text file and image format are available at http://dx.doi.org/10.25532/OPARA-277 (Loebel et al., 2023a).

5 Conclusions

Accurate as well as temporally and spatially comprehensive calving front data is essential for understanding and modelling glacial evolution. This paper addresses this requirement and presents a new data record for glaciers at the AP. The data is generated by applying multispectral Landsat-8 and Landsat-9 imagery to a deep learning based processing system. We validated the processing system for accuracy, robustness, and generalization capabilities using independent test data. The mean difference between automated and manual extraction $59.3 \pm 5.9\,\mathrm{m}$. The resulting data record contains 2604 calving front locations for 19 key outlet glaciers from 2013 to 2023. It achieves sub-seasonal temporal resolution for all of the processed glaciers.

https://doi.org/10.5194/essd-2023-535
Preprint. Discussion started: 2 February 2024

More broadly, this contribution exemplifies that well generalised ANN processing systems can be applied to various regions of interest with only minor additions to reference data. With over 3000 marine-terminating glaciers worldwide (RGI Consortium, 2017), this is particularly relevant for extracting calving fronts. We expect that our presented data record will not only advance glaciological research for the AP, but also contribute to future deep learning based calving front data products and data inter-comparison projects.

Author contributions. EL applied the processing system, did the accuracy assessment and carried out the data product generation. CAB, AD and MS provided direction for the study and supervised the work. EL prepared the paper with contributions from CAB, MH and MS. AD and MS acquired funding for this research.

Competing interests. The author declares that there are no competing interests.

Acknowledgements. We thank the USGS for providing Landsat-8 and Landsat-9 imagery. We are grateful to the TU Dresden computing centre (ZIH) for providing their high-performance and storage infrastructure. We acknowledge the Norwegian Polar Institute's Quantarctica package. This work was supported by the Helmholtz Association of German Research Centers as part of the Helmholtz Information and Data Science Incubator, project "Artificial Intelligence for Cold Regions" (AI-CORE, grant no. ZT-I-0016), and by the German Federal Ministry of Education and Research (BMBF), project "Greenland Ice Sheet/Ocean Interaction" (GROCE2, grant no. 03F0778G).

https://doi.org/10.5194/essd-2023-535
Preprint. Discussion started: 2 February 2024

References

Adusumilli, S., Fricker, H. A., Siegfried, M. R., Padman, L., Paolo, F. S., and Ligtenberg, S. R.: Variable basal melt rates of Antarctic Peninsula ice shelves, 1994–2016, Geophysical Research Letters, 45, 4086–4095, https://doi.org/10.1002/2017GL076652, 2018.

Alley, R. B., Clark, P. U., Huybrechts, P., and Joughin, I.: Ice-sheet and sea-level changes, science, 310, 456–460, https://doi.org/10.1126/science.1114613, 2005.

Barrand, N. E., Hindmarsh, R. C., Arthern, R. J., Williams, C. R., Mouginot, J., Scheuchl, B., Rignot, E., Ligtenberg, S. R., Van Den Broeke, M. R., Edwards, T. L., et al.: Computing the volume response of the Antarctic Peninsula ice sheet to warming scenarios to 2200, Journal of Glaciology, 59, 397–409, https://doi.org/10.3189/2013JoG12J139, 2013.

Baumhoer, C. A., Dietz, A. J., Kneisel, C., and Kuenzer, C.: Automated Extraction of Antarctic Glacier and Ice Shelf Fronts from Sentinel-1 Imagery Using Deep Learning, Remote Sensing, 11, 2529, https://doi.org/10.3390/rs11212529, 2019.

Baumhoer, C. A., Dietz, A. J., Heidler, K., and Kuenzer, C.: IceLines–A new data set of Antarctic ice shelf front positions, Scientific Data, 10, 138, 2023.

Cape, M., Vernet, M., Skvarca, P., Marinsek, S., Scambos, T., and Domack, E.: Foehn winds link climate-driven warming to ice shelf evolution in Antarctica, Journal of Geophysical Research: Atmospheres, 120, 11–037, https://doi.org/10.1002/2015JD023465, 2015.

Cheng, D., Hayes, W., Larour, E., Mohajerani, Y., Wood, M., Velicogna, I., and Rignot, E.: Calving Front Machine (CALFIN): Glacial Termini Dataset and Automated Deep Learning Extraction Method for Greenland, 1972–2019 , The Cryosphere, 15, https://doi.org/10.5194/tc-15-1663-2021, 2021.

Cook, A., Fox, A., and Thomson, J.: Coastal change data for the Antarctic Peninsula region, 1843 to 2008 (Version 1.0) [Data set], https://doi.org/10.5285/07727663-9B94-4069-A486-67E4D82177D3, 2021.

Cook, A. J. and Vaughan, D. G.: Overview of areal changes of the ice shelves on the Antarctic Peninsula over the past 50 years, The cryosphere, 4, 77–98, https://doi.org/10.5194/tc-4-77-2010, 2010.

Cook, A. J., Fox, A. J., Vaughan, D. G., and Ferrigno, J. G.: Retreating Glacier Fronts on the Antarctic Peninsula over the Past Half-Century, Science, 308, 541–544, https://doi.org/10.1126/science.1104235, 2005.

Cook, A. J., Holland, P., Meredith, M., Murray, T., Luckman, A., and Vaughan, D. G.: Ocean forcing of glacier retreat in the western Antarctic Peninsula, Science, 353, 283–286, https://doi.org/10.1126/science.aae0017, 2016.

Cornford, S. L., Martin, D., Payne, A., Ng, E., Le Brocq, A., Gladstone, R. M., Edwards, T. L., Shannon, S. R., Agosta, C., van den Broeke, M. R., et al.: Century-scale simulations of the response of the West Antarctic Ice Sheet to a warming climate, The Cryosphere, 9, 1579–1600, https://doi.org/10.5194/tc-9-1579-2015, 2015.

Davari, A., Baller, C., Seehaus, T., Braun, M., Maier, A., and Christlein, V.: Pixelwise Distance Regression for Glacier Calving Front Detection and Segmentation, IEEE Transactions on Geoscience and Remote Sensing, 60, 1–10, https://doi.org/10.1109/TGRS.2022.3158591, 2022a.

Davari, A., Islam, S., Seehaus, T., Hartmann, A., Braun, M., Maier, A., and Christlein, V.: On Mathews Correlation Coefficient and Improved Distance Map Loss for Automatic Glacier Calving Front Segmentation in SAR Imagery, IEEE Transactions on Geoscience and Remote Sensing, 60, 1–12, https://doi.org/10.1109/TGRS.2021.3115883, 2022b.

Davies, B. J., Hambrey, M. J., Smellie, J. L., Carrivick, J. L., and Glasser, N. F.: Antarctic Peninsula ice sheet evolution during the Cenozoic Era, Quaternary Science Reviews, 31, 30–66, https://doi.org/https://doi.org/10.1016/j.quascirev.2011.10.012, 2012.

ENVEO: Ice Flow and Calving Front – Timeseries, https://cryoportal.enveo.at/iv/calvingfront/, accessed: 2023-09-08.

Friedl, P., Seehaus, T. C., Wendt, A., Braun, M. H., and Höppner, K.: Recent dynamic changes on Fleming Glacier after the disintegration of Wordie Ice Shelf, Antarctic Peninsula, The Cryosphere, 12, 1347–1365, https://doi.org/10.5194/tc-12-1347-2018, 2018.

GDAL/OGR contributors: GDAL/OGR Geospatial Data Abstraction software Library, Open Source Geospatial Foundation, https://gdal.org, 2020.

GLIMS Consortium, .: GLIMS Glacier Database, Version 1, https://doi.org/10.7265/N5V98602, 2005.

Goliber, S., Black, T., Catania, G., Lea, J. M., Olsen, H., Cheng, D., Bevan, S., Bjørk, A., Bunce, C., Brough, S., Carr, J. R., Cowton, T., Gardner, A., Fahrner, D., Hill, E., Joughin, I., Korsgaard, N. J., Luckman, A., Moon, T., Murray, T., Sole, A., Wood, M., and Zhang, E.: TermPicks: a century of Greenland glacier terminus data for use in scientific and machine learning applications, The Cryosphere, 16, 3215–3233, https://doi.org/10.5194/tc-16-3215-2022, 2022.

Gourmelon, N., Seehaus, T., Braun, M., Maier, A., and Christlein, V.: Calving fronts and where to find them: a benchmark dataset and methodology for automatic glacier calving front extraction from synthetic aperture radar imagery, Earth System Science Data, 14, 4287–4313, https://doi.org/10.5194/essd-14-4287-2022, 2022.

Gourmelon, N., Seehaus, T., Braun, M. H., Maier, A., and Christlein, V.: CaFFe (CAlving Fronts and where to Find thEm: a benchmark dataset and methodology for automatic glacier calving front extraction from sar imagery) [Data set], https://doi.org/10.1594/PANGAEA.940950, 2022.

Heidler, K., Mou, L., Baumhoer, C., Dietz, A., and Zhu, X. X.: HED-UNet: Combined Segmentation and Edge Detection for Monitoring the Antarctic Coastline, IEEE Transactions on Geoscience and Remote Sensing, 2021.

Heidler, K., Mou, L., Loebel, E., Scheinert, M., Lefèvre, S., and Zhu, X. X.: Deep Active Contour Models for Delineating Glacier Calving Fronts, in: IGARSS 2022 - 2022 IEEE International Geoscience and Remote Sensing Symposium, pp. 4490–4493, https://doi.org/10.1109/IGARSS46834.2022.9884819, 2022.

Herrmann, O., Gourmelon, N., Seehaus, T., Maier, A., Fürst, J. J., Braun, M. H., and Christlein, V.: Out-of-the-box calving-front detection method using deep learning, The Cryosphere, 17, 4957–4977, https://doi.org/10.5194/tc-17-4957-2023, 2023.

Kingma, D. P. and Ba, J.: Adam: A Method for Stochastic Optimization, arXiv preprint arXiv:1412.6980, 2014.

Li, T., Heidler, K., Mou, L., Ignéczi, A., Zhu, X. X., and Bamber, J. L.: A High-Resolution Calving Front Data Product for Marine-Terminating Glaciers in Svalbard, Earth System Science Data Discussions, 2023, 1–28, https://doi.org/10.5194/essd-2023-396, 2023.

Lippl, S.: Glacier Surface Velocities and Outlet Areas from 2014-2018 on James Ross Island, Northern Antarctic Peninsula [Data set], https://doi.org/10.1594/PANGAEA.907062, supplement to: Lippl, Stefan; Friedl, Peter; Kittel, Christoph; Marinsek, Sebastián; Seehaus, Thorsten; Braun, Matthias Holger (2019): Spatial and Temporal Variability of Glacier Surface Velocities and Outlet Areas on James Ross Island, Northern Antarctic Peninsula. Geosciences, 9(9), 374, https://doi.org/10.3390/geosciences9090374, 2019.

Loebel, E.: eloebel/glacier-front-extraction: Initial release v1.0.0 [code], Zenodo, https://doi.org/10.5281/zenodo.7755774, 2023a.

Loebel, E.: eloebel/rectilinear-box-method: Initial release v1.0.0 [code], Zenodo, https://doi.org/10.5281/zenodo.7738605, 2023b.

Loebel, E., Scheinert, M., Horwath, M., Heidler, K., Christmann, J., Phan, L. D., Humbert, A., and Zhu, X. X.: Extracting Glacier Calving Fronts by Deep Learning: The Benefit of Multispectral, Topographic, and Textural Input Features, IEEE Transactions on Geoscience and Remote Sensing, 60, 1–12, https://doi.org/10.1109/TGRS.2022.3208454, 2022.

Loebel, E., Baumhoer, C. A., Dietz, A., Scheinert, M., and Horwath, M.: Terminus area change of 17 key glaciers of the Antarctic Peninsula from 2013 to 2023 derived from remote sensing and deep learning [data set], TU Dresden OpARA, https://doi.org/http://dx.doi.org/10.25532/OPARA-277, 2023a.

Loebel, E., Baumhoer, C. A., Dietz, A., Scheinert, M., and Horwath, M.: Glacier calving front locations for the Antarctic Peninsula derived from remote sensing and deep learning from 2013 to 2023 [Data set], https://doi.pangaea.de/10.1594/PANGAEA.963725, 2023b.

Loebel, E., Scheinert, M., Horwath, M., Humbert, A., Sohn, J., Heidler, K., Liebezeit, C., and Zhu, X. X.: Calving front monitoring at sub-seasonal resolution: a deep learning application to Greenland glaciers, The Cryosphere Discussions, 2023, 1–21, 2023c.

Marochov, M., Stokes, C. R., and Carbonneau, P. E.: Image classification of marine-terminating outlet glaciers in Greenland using deep learning methods, The Cryosphere, 15, 5041–5059, https://doi.org/10.5194/tc-15-5041-2021, 2021.

Mohajerani, Y., Wood, M., Velicogna, I., and Rignot, E.: Detection of Glacier Calving Margins with Convolutional Neural Networks: A Case Study , Remote Sensing, 11, 74, https://doi.org/10.3390/rs11010074, 2019.

Moon, T. and Joughin, I.: Changes in ice front position on Greenland's outlet glaciers from 1992 to 2007, Journal of Geophysical Research: Earth Surface, 113, https://doi.org/10.1029/2007JF000927, 2008.

Ochwat, N. E., Scambos, T. A., Banwell, A. F., Anderson, R. S., Maclennan, M. L., Picard, G., Shates, J. A., Marinsek, S., Margonari, L., Truffer, M., and Pettit, E. C.: Triggers of the 2022 Larsen B multi-year landfast sea ice break-out and initial glacier response, The Cryosphere Discussions, 2023, 1–34, https://doi.org/10.5194/tc-2023-88, 2023.

Otosaka, I. N., Shepherd, A., Ivins, E. R., Schlegel, N.-J., Amory, C., van den Broeke, M. R., Horwath, M., Joughin, I., King, M. D., Krinner, G., Nowicki, S., Payne, A. J., Rignot, E., Scambos, T., Simon, K. M., Smith, B. E., Sørensen, L. S., Velicogna, I., Whitehouse, P. L., A, G., Agosta, C., Ahlstrøm, A. P., Blazquez, A., Colgan, W., Engdahl, M. E., Fettweis, X., Forsberg, R., Gallée, H., Gardner, A., Gilbert, L., Gourmelen, N., Groh, A., Gunter, B. C., Harig, C., Helm, V., Khan, S. A., Kittel, C., Konrad, H., Langen, P. L., Lecavalier, B. S., Liang, C.-C., Loomis, B. D., McMillan, M., Melini, D., Mernild, S. H., Mottram, R., Mouginot, J., Nilsson, J., Noël, B., Pattle, M. E., Peltier, W. R., Pie, N., Roca, M., Sasgen, I., Save, H. V., Seo, K.-W., Scheuchl, B., Schrama, E. J. O., Schröder, L., Simonsen, S. B., Slater, T., Spada, G., Sutterley, T. C., Vishwakarma, B. D., van Wessem, J. M., Wiese, D., van der Wal, W., and Wouters, B.: Mass balance of the Greenland and Antarctic ice sheets from 1992 to 2020, Earth System Science Data, 15, 1597–1616, https://doi.org/10.5194/essd-15-1597-2023, 2023.

Periyasamy, M., Davari, A., Seehaus, T., Braun, M., Maier, A., and Christlein, V.: How to Get the Most Out of U-Net for Glacier Calving Front Segmentation, IEEE Journal of Selected Topics in Applied Earth Observations and Remote Sensing, 15, 1712–1723, https://doi.org/10.1109/JSTARS.2022.3148033, 2022.

Rack, W. and Rott, H.: Pattern of retreat and disintegration of the Larsen B ice shelf, Antarctic Peninsula, Annals of glaciology, 39, 505–510, https://doi.org/10.3189/172756404781814005, 2004.

RGI Consortium: Randolph Glacier Inventory - A Dataset of Global Glacier Outlines, Version 6, https://doi.org/10.7265/4m1f-gd79, 2017.

Rignot, E., Casassa, G., Gogineni, P., Krabill, W., Rivera, A., and Thomas, R.: Accelerated ice discharge from the Antarctic Peninsula following the collapse of Larsen B ice shelf, Geophysical research letters, 31, https://doi.org/10.1029/2004GL020697, 2004.

Ronneberger, O., Fischer, P., and Brox, T.: U-Net: Convolutional Networks for Biomedical Image Segmentation, In: Navab N., Hornegger J., Wells W., Frangi A. (eds) Medical Image Computing and Computer-Assisted Intervention – MICCAI 2015., 9351, 234–241, https://doi.org/10.1007/978-3-319-24574-4_28, 2015.

Rott, H., Skvarca, P., and Nagler, T.: Rapid collapse of northern Larsen ice shelf, Antarctica, Science, 271, 788–792, https://doi.org/10.1126/science.271.5250.788, 1996.

Rott, H., Abdel Jaber, W., Wuite, J., Scheiblauer, S., Floricioiu, D., Van Wessem, J. M., Nagler, T., Miranda, N., and Van Den Broeke, M. R.: Changing pattern of ice flow and mass balance for glaciers discharging into the Larsen A and B embayments, Antarctic Peninsula, 2011 to 2016, The Cryosphere, 12, 1273–1291, https://doi.org/10.5194/tc-12-1273-2018, 2018.

Scambos, T. A., Berthier, E., and Shuman, C. A.: The triggering of subglacial lake drainage during rapid glacier drawdown: Crane Glacier, Antarctic Peninsula, Annals of Glaciology, 52, 74–82, https://doi.org/https://doi.org/10.3189/172756411799096204, 2011.

Seehaus, T., Marinsek, S., Helm, V., Skvarca, P., and Braun, M.: Changes in ice dynamics, elevation and mass discharge of Dinsmoor–Bombardier–Edgeworth glacier system, Antarctic Peninsula, Earth and Planetary Science Letters, 427, 125–135, https://doi.org/https://doi.org/10.1016/j.epsl.2015.06.047, 2015.

Seehaus, T., Marinsek, S., Helm, V., Skvarca, P., and Braun, M. H.: Surface velocity fields, digital elevation models, ice front positions and grounding line derived from remote sensing data at Dinsmoor-Bombardier-Edgeworth glacier system, Antarctic Peninsula (1992-2014) [Data set], https://doi.org/10.1594/PANGAEA.859573, supplement to: Seehaus, T et al. (2015): Changes in ice dynamics, elevation and mass discharge of Dinsmoor-Bombardier-Edgeworth glacier system, Antarctic Peninsula. Earth and Planetary Science Letters, 427, 125-135, https://doi.org/10.1016/j.epsl.2015.06.047, 2015.

Seehaus, T., Marinsek, S., Skvarca, P., van Wessem, J. M., Tijm-Reijmer, C. H., Seco, J., and Braun, M. H.: Surface velocity fields, digital elevation models and ice front positions derived from multi-mission SAR remote sensing data at Sjögren Inlet glaciers, Antarctic Peninsula [Data set], https://doi.org/10.1594/PANGAEA.859255, supplement to: Seehaus, T et al. (2016): Dynamic response of Sjögren Inlet glaciers, Antarctic Peninsula, to ice shelf breakup derived from multi-mission remote sensing time series. Frontiers in Earth Science Section; Section: Cryospheric Sciences, 4(66), 1-13, https://doi.org/10.3389/feart.2016.00066, 2016.

Seehaus, T., Cook, A. J., Silva, A. B., and Braun, M.: Changes in glacier dynamics in the northern Antarctic Peninsula since 1985, The Cryosphere, 12, 577–594, https://doi.org/https://doi.org/10.5194/tc-12-577-2018, 2018.

Seehaus, T., Sommer, C., Dethinne, T., and Malz, P.: Mass changes of the northern Antarctic Peninsula Ice Sheet derived from repeat bi-static synthetic aperture radar acquisitions for the period 2013–2017, The Cryosphere, 17, 4629–4644, https://doi.org/10.5194/tc-17-4629-2023, 2023.

Seehaus, T. C., Marinsek, S., Skvarca, P., Van Wessem, J. M., Reijmer, C. H., Seco, J. L., and Braun, M. H.: Dynamic response of sjögren inlet glaciers, antarctic peninsula, to ice shelf breakup derived from multi-mission remote sensing time series, Frontiers in Earth Science, 4, 66, https://doi.org/https://doi.org/10.3389/feart.2016.00066, 2016.

Slater, T., Hogg, A. E., and Mottram, R.: Ice-sheet losses track high-end sea-level rise projections, Nature Climate Change, 10, 879–881, https://doi.org/10.1038/s41558-020-0893-y, 2020.

Vaughan, D. G. and Doake, C. S.: Recent atmospheric warming and retreat of ice shelves on the Antarctic Peninsula, Nature, 379, 328–331, https://doi.org/10.1038/379328a0, 1996.

Wallis, B. J., Hogg, A. E., van Wessem, J. M., Davison, B. J., and van den Broeke, M. R.: Widespread seasonal speed-up of west Antarctic Peninsula glaciers from 2014 to 2021, Nature Geoscience, 16, 231–237, https://doi.org/https://doi.org/10.1038/s41561-023-01131-4, 2023a.

Wallis, B. J., Hogg, A. E., van Wessem, J. M., and van den Broeke, M.: Data for Widespread seasonal speed-up of west Antarctic Peninsula glaciers from 2014-2021, https://doi.org/10.5281/zenodo.7521416, 2023b.

Zhang, E., Liu, L., Huang, L., and Ng, K. S.: An automated, generalized, deep-learning-based method for delineating the calving fronts of Greenland glaciers from multi-sensor remote sensing imagery, Remote Sensing of Environment, 254, 112 265, https://doi.org/10.1016/j.rse.2020.112265, 2021.

Zhang, E., Catania, G., and Trugman, D. T.: AutoTerm: an automated pipeline for glacier terminus extraction using machine learning and a “big data” repository of Greenland glacier termini, The Cryosphere, 17, 3485–3503, https://doi.org/10.5194/tc-17-3485-2023, 2023.